Applied Surface Science 405 (2017) 321–328

Contents lists available at ScienceDirect

Applied Surface Science

journal homepage: www.elsevier.com/locate/apsusc

Full Length Article

Double positive effect of adding hexaethyelene glycol when optimizing the hybridization efficiency of a microring DNA detection assay

Anabelle Van Eeghem[a,b,*], Sam Werquin[b,c], Jan-Willem Hoste[b,c,*], Arne Goes[a,d], Els Vanderleyden[a,b], Peter Bienstman[b,c], Peter Dubruel[a,b]

[a] Polymer Chemistry and Biomaterials Research Group, Department of Organic and Macromolecular Chemistry, Ghent University, Belgium
[b] Center for Nano- and Biophotonics, Ghent University, Belgium
[c] Photonics Research Group, Department of Information Technology, Ghent University – IMEC, Belgium
[d] Agrosavfe NV, Technologiepark 4 (Bio-incubator), Zwijnaarde, Belgium

ARTICLE INFO

Article history:
Received 16 August 2016
Received in revised form 27 January 2017
Accepted 9 February 2017
Available online 11 February 2017

Keywords:
Surface functionalization
DNA detection
Microring resonator
Non-specific binding
Backfilling
Probe orientation

ABSTRACT

In this paper, a method for detection of DNA molecules using silicon-on-insulator (SOI) microring resonators is described. The influence of temperature and the use of formamide on the hybridization efficiency were studied. It was shown that 50 v/v% of formamide in the hybridization buffer can ensure hybridization when working close to physiological temperature. Furthermore, the use of hexaethylene glycol (HEG) as backfilling agent was studied in order to resolve issues of non-specific adsorption to the surface. The results indicated that not only non-specific binding was reduced significantly but also that HEG improves the orientation of the DNA probes on the surface. This led to a 4-fold increase in hybridization efficiency and thus in an equal decrease in the detection limit, compared to hybridization without the use of HEG. An improvement in robustness of the assay was also observed. This DNA reorientation hypothesis was confirmed by studying the thickness and density of the layers by using dual polarization microring sensing. Finally, the different steps in the sensing experiment were characterized in more detail by static contact angle (SCA) and X-ray photoelectron spectroscopy (XPS) analysis. The results showed quantitatively that the surface modifications were successful.

1. Introduction

In the last decade, a growing interest in detection of biomolecules, e.g. proteins or oligonucleotides, can be observed in several research fields, such as food safety [1], medical diagnostics [2–4] and drug development [5]. A major problem in today's healthcare is the increasing resistance of bacteria against antibiotics. The use of medical diagnostics, such as point-of-care (POC) tests, can help clinicians to make decisions in a fast and reliable way, which will lead to a lower use of antibiotics [6]. The key component of such a POC test is a biosensor that provides specific and rapid results. In the field of biosensors, two main classes, label-based and label-free biosensors, can be distinguished.

The principle of label-based detection consists of the binding of a label (e.g. protein, antibody) to the previously immobilized target. This label can bind specifically or non-specifically and is often fluorescent to facilitate visualization of the signal [7]. This indirect sensing method has the important drawback that no real-time information can be obtained [8] and multiplexing is rather complicated [9]. Both of these issues can be overcome with label-free biosensors. The most common label-free detection technology is surface plasmon resonance (SPR). In this paper, silicon-on-insulator (SOI) microring resonators were selected as detection platform. They combine a comparable performance as SPR [10] with the possibility of multiplexing and low cost due to mass production of silicon wafers [11]. The microring detection platform has been used to study a wide variety of biological entities. It has found widespread use in the field of proteomics where assays have been made that detect a protein using a specific antibody on the resonator surface [12–14]. Successful detection of nucleotides has been reported in the form of DNA assays [15] as well as microRNA assays [16]. Furthermore the detection of small biomolecules such

* Corresponding authors at: Center for Nano- and Biophotonics, Ghent University, Belgium.
E-mail addresses: anabelle.vaneeghem@gmail.com (A. Van Eeghem), janwillem.hoste@ugent.be (J.-W. Hoste).

http://dx.doi.org/10.1016/j.apsusc.2017.02.064
0169-4332/

as glucose has been demonstrated [17], as well as larger entities such as viruses [18] and bacteria [19]. Wang et al. have studied cell growth using this platform [20]. Work has also been done to apply the microring resonator in the field of microforce sensing [21] or seismic sensing [22]. In this paper, we present an assay for the detection of target DNA molecules via ring resonators. The SOI surface was coated with a silicon nitride layer to ensure the reproducibility of the experiments. Indeed, previous studies have shown that in some cases surface modifications, such as silanization, can be more efficient on the area next to optical waveguides then on the waveguides themselves [23]. This is due to the use of different etchants during the production process of the silicon wafers. The silicon nitride layer that we chose to add excludes the influence of these etchants. In this paper, we want to investigate the impact of different hybridization conditions, buffer, temperature and backfilling prior to hybridization, on the detection efficiency. Immobilization of a capture DNA probe onto the SOI surface was done following the strategy developed by Byeon et al. using the commercially available reagents HyNic Silane and S-4FB [24,25]. After the immobilization of a DNA capture probe to the surface, a complementary DNA sequence, the target, was hybridized and detected. Hybridization conditions were optimized by varying conditions such as hybridization buffer and temperature. Furthermore, the surface is prone to non-specific adsorption of biomolecules. Several blocking agents to circumvent this problem are reported in literature, such as bovine serum albumin (BSA) [26] or polymers [27]. The use of poly(ethylene glycol) (PEG) derivatives is widespread in non-fouling applications [28–31]. In this study, the PEG approach was applied via a backfilling method [32]. For this reason, a short PEG chain, hexa(ethylene glycol) (HEG), was chosen in order to allow the chains to adsorb to the surface in between the previously immobilized DNA probes. The orientation of these probes and the influence of the HEG layer were studied via the dual polarization microring technique [33]. Finally, the observations of the ring resonator experiments were verified via XPS and SCA analysis.

2. Materials and methods

2.1. Materials

Ethanol (EtOH), 3-N-((6-(N′-Isopropylidene-hydrazino))nicotinamide)propyltriethyoxysilane (HyNic Silane, Solulink) and succinimidyl 4-formylbenzoate (sulfo-S-4FB, Solulink) were purchased from VWR (Leuven, Belgium). Dimethylformamide (DMF), aniline, formamide and hexaethylene glycol (HEG) were supplied by Sigma-Aldrich (Bornem, Belgium). DNA probe 1 (5′-CTCTCTCTCTCTCTCTCTCATGAGTCGTGAGTACGCTT-3′) and DNA probe 2, containing a hexaethylene glycol spacer between the 5′-end and the DNA sequence, were purchased at Eurogentec (Seraing, Belgium) and Integrated DNA Technologies (Leuven, Belgium), respectively. Both were amino-modified at the 5′- end. The complementary DNA (5′-CTCCTCA GTAATAGTGTCTTACAAGCGTACTCACGACTCATGAAATCG-CCGGACTGCCGGTGGTCGACAGGTCGGTGTATGCAG-3′) was prepared by rolling circle amplification [34] and delivered by SciLifeLab (Uppsala, Sweden).

2.2. Detection of DNA using ring resonator SOI chips

The SOI chips, equipped with 64 ring resonators, were supplied by imec (Leuven, Belgium) and coated with a silicon nitride layer (SiNx) of 9 nm using a plasma-enhanced chemical vapor deposition (PECVD) device. The ring resonators were illuminated using a Santec TSL-510 tunable laser, while the emitted light was detected using a Xenics Xeva-1.7.320 infrared camera mounted on an optical microscope. During the experiment, the liquid was flowed over the chip at a constant flow rate of 5 μl/min. A SEM picture of the ring resonator devices used for DNA detection is shown in Fig. 1. The devices have a radius of 20 μm and the waveguide of the ring resonator has a width of 450 nm and a thickness of 220 nm. Light is coupled in and out via vertical grating couplers routed to the left and right of the device. The coupling section, which is crucial for the device operation, is illustrated in the bottom left of the figure.

2.2.1. Silanization

The sensor chip was activated by a low pressure plasma treatment (Diener Femto) with oxygen during 5 min. Next, the surface was rinsed with EtOH to obtain a stable binding curve. A solution of 2 v/v% HyNic Silane in 95% EtOH and 5% DMF is flowed over the ring resonators. After 20 min reaction, the surface was rinsed with EtOH again.

2.2.2. DNA probe attachment

Prior to coupling, the DNA recognition probe was modified with sulfo-S-4FB via the amino group at the 5′-end. This approach has been described in literature for the modification of antibodies [24] and single-stranded DNA [25] with an aldehyde. After modification, the DNA solution was stored at −20 °C before coupling to the silicon surface.

After the silanization step, the surface was rinsed with a solution containing 1 mM phosphate buffered saline (PBS) pH 6 and 100 mM aniline. A 1 μM solution of DNA probe 1 or DNA probe 2 was flowed over the sensors during 40 min, followed by rinsing with the buffer.

2.2.3. Backfilling

When DNA probe 2 was attached to the surface, a solution of HEG, with concentrations varying from 0.01 to 10 mg/ml in PBS pH 6, was flowed over the sensors during 40 min.

2.2.4. Hybridization

A 10 nM solution of complementary DNA in hybridization buffer was flowed over the ring resonators. The hybridization buffer was composed of 10 mM PBS pH 7.4 and 25 v/v% or 50 v/v% of formamide. Hybridization experiments were performed both at room temperature and at 35 °C. The surface was rinsed with hybridization buffer after 40 min of hybridization.

2.3. Determination of layer thickness and density by dual polarization experiments

The experiments described in Section 2.2 were repeated using dual polarization SOI chips [33]. The microrings on these chips are designed in such a way that both the fundamental transverse electric (TE) and the fundamental transverse magnetic (TM) mode are excited simultaneously in the microring cavity. Tracking the resonant wavelength of both modes allows to characterize the geometry of the thin bound layer by determining its thickness and density separately, as opposed to only being able to measure the product of the two, i.e. the total adsorbed mass, when using a microring excited with a single mode. Using both modes thus allows one to gain additional conformational information. This technique was used to study the influence of the HEG molecules on the spatial organization of the DNA probes. In order to do so, the microring surface was silanized and after attachment of DNA probe 2, the surface was backfilled with a 1 mg/ml HEG solution. It is important to realize that the outcome of the experiment is dependent on the knowledge we have on the thickness and refractive index of the silicon surface. As such, a shorter plasma step of 0.4 min in air was performed, to not create a significant oxide layer of unknown thickness and refractive index. The deposited nitride

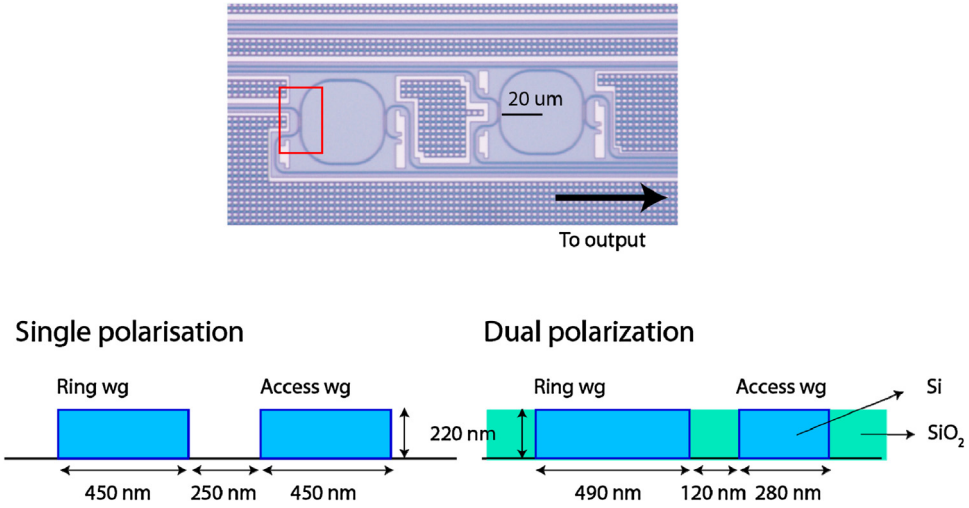

Fig. 1. SEM picture of the microring device. The coupling section in the red rectangle is illustrated in cross section at the bottom for both the single polarization ring resonator as for the dual polarization ring resonator. For both devices, the radius equals 20 μm. We see that the dual polarization exhibits an asymetrical coupling section used to excite both TE and TM mode simultaneously in the ring resonator [33]. The single polarisation resonator exhibits a conventional coupling section. (For interpretation of the references to colour in this figure legend, the reader is referred to the web version of this article.)

layer was characterized as an 8 nm thick layer with refractive index of 1.9348 at 1565 nm by ellipsometry. Finally, the waveguides on this chip are planarized, meaning that only the top surface of the silicon waveguide is accessible for the analytes. The sidewalls of the waveguide are thus covered with silicon dioxide. Although this reduces the response of the TE mode in size, it does simplify the complicated solving algorithms to translate the shifts of both modes to a thickness and density profile of the bound layer, which outweighs the reduced TE response. From a surface chemistry viewpoint, a planar surface is advantageous as well. The device structure is similar to the ring resonators used for the DNA detection experiments shown in Fig. 1. The radius equals 20 μm as well. An important difference is the width of the waveguide of the ring resonator and the design of the coupling section, illustrated in the bottom right of the figure. The coupling section is designed such that the TE mode of the access waveguide excites both the TE and the TM mode of the ring waveguide simultaneously. This is further described in [33].

2.4. Surface characterization methods

In order to characterize the surface modifications steps on the SOI chips, the procedure described in section 2.2 was performed on silicon nitride-coated flat silicon wafers under static conditions. The silicon samples were immersed in the appropriate solutions and after each step, a sample was collected and rinsed with the corresponding buffer. Both DNA probes and backfilling with 1 mg/ml HEG were tested.

2.4.1. Static contact angle (SCA)

An OCA 20 device (Dataphysics, distributed by Benelux Scientific) was used to perform SCA measurements on the silicon nitride coated samples. With a 500 μl Hamilton syringe, droplets of 1 μl of double distilled water were placed on the surfaces. A video camera was used to image the droplets, after which the contact angles were determined using the imaging software provided by the supplier (SCA 20, version 2.1.5 build 16). The SCA measurements were performed in triplicate.

2.4.2. X-ray photoelectron spectroscopy (XPS)

XPS measurements were performed on the silicon nitride using a FISONS S-PROBE, a dedicated XPS instrument designed for high-end analysis performance while providing a high sample throughput. Compared to conventional twin anode sources, a lower background and higher sensitivity are obtained thanks to the fine focus Al-Kα source with a quartz monochromator, developed by Fisons Instruments Surface Science. All measurements were performed in a vacuum of at least 10^{-9} Pa. Wide scan spectra were acquired at pass energy of 158 eV. The binding energy was calibrated by the C 1s peak at 285 eV. The spot size used was 250 μm on 1 mm. Data analysis was performed using S-PROBE software. The measured spectrum was displayed as a plot of the number of electrons (electron counts) versus electron binding energy in a fixed, small energy interval. Peak area and peak height sensitivity factors were used for the quantifications. All surface compositions in this work are expressed as atomic percentages (at%). XPS analysis was performed in triplicate.

Table 1
Resonance wavelength shift observed after backfilling and hybridization in function of HEG concentration.

HEG concentration (mg/ml)	backfilling wavelength shift (pm)	hybridization wavelength shift (pm)
0.00	–	85.8 ± 36.9
0.01	11.1 ± 7.8	41.4 ± 32.4
0.05	8.4 ± 4.0	41.9 ± 26.1
0.10	11.0 ± 4.2	381.7 ± 21.0
1.00	19.9 ± 8.2	361.0 ± 22.0
10.00	46.3 ± 7.6	325.6 ± 53.8

2.5. Statistical analysis

Statistical analysis, using the Student *t*-test, was performed on the wavelength shifts of Table 1 and on the SCA and XPS results. Two values were considered significantly different when $p < 0.05$.

3. Results and discussion

3.1. Detection of DNA using ring resonator SOI chips

3.1.1. Silanization and coupling of the DNA probe to the surface

During the experiments, real-time binding curves are obtained indicating the resonance wavelength. After each step, a net wavelength shift can be deducted from each binding curve. Fig. 2(a)

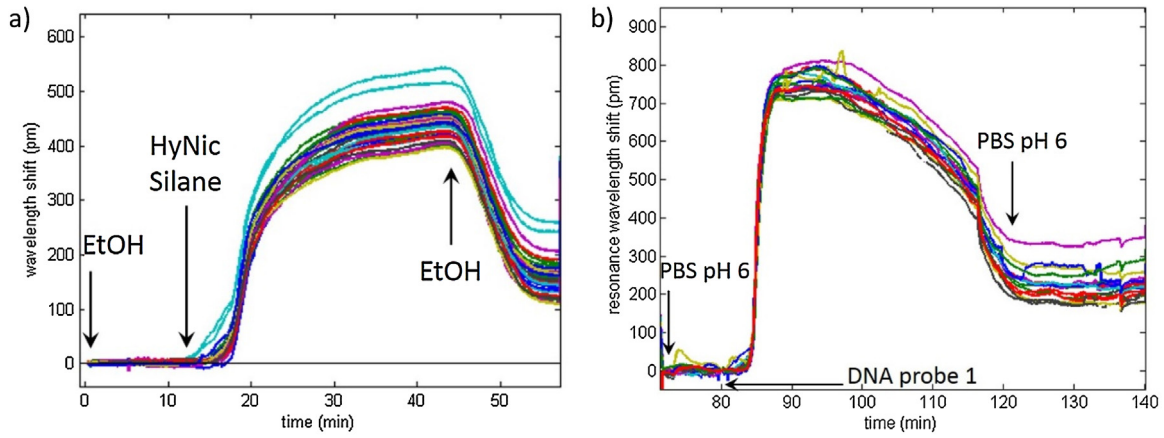

Fig. 2. Binding curve showing the resonance wavelenght shift during (a) the silanization step and (b) coupling of the DNA probe to the surface. An net wavelenght shift ranging from 100 to 300 pm (a) and 200–400 pm (b) was obtained.

shows the binding curve of the silanization step. The initial flow of EtOH results in a stable response. Immediately after the injection of the HyNic Silane solution, a steep increase of the wavelength is observed. During reaction, this increase becomes gradual and when EtOH is flowed again over the resonators, the wavelength will partially decrease again, indicating that physically adsorbed molecules are being washed away. The resulting net wavelength shift ranges from 100 to 300 pm for the different sensors, indicating that the silanization step was successful. A similar binding curve, shown in Fig. 2(b), was obtained for the next step, the coupling of the DNA probe to the surface. In this case, the net wavelength shift ranges from 200 to 400 pm.

3.1.2. Optimization of hybridization by varying hybridization buffer and temperature

The hybridization protocol applied in these experiments is based on a procedure described by Qavi and Bailey [35], where a hybridization buffer containing 50 v/v% formamide in PBS pH 7.4 is used for detection of miRNAs. The concentration of formamide in the hybridization buffer was varied, both 25 v/v% and 50 v/v% were tested. To investigate the effect of hybridization close to physiological temperature, experiments were performed both at room temperature and at 35 °C.

At room temperature, no hybridization was observed when using both hybridization buffers (data not shown). When working at 35 °C, hybridization was observed in some experiments with the hybridization buffer containing 25 v/v% formamide, although the results were not reproducible. Moreover, a negative drift of the wavelength was observed when washing the surface with buffer, indicating that the hybridization was either not successful or not permanent. A binding curve of a hybridization experiment at these conditions is shown in Fig. 3(a). The average shift amounts to $6{\cdot}10^1$ pm with a relative standard deviation of 0.7. On the other hand, when using the hybridization buffer containing 50 v/v% formamide, reproducible results were obtained and an average resonance wavelength shift of $8{\cdot}10^1$ pm was obtained after hybridization, with a relative standard deviation of 0.1, as can be seen in Fig. 3(b). The relative standard deviation can be interpreted as a measure for robustness of the biological assay, since the curves of one graph represent different sensors on the same chip, subject to the same biochemical processing steps. The improvement of the relative standard deviation of 0.7–0.1 indicates that changing the concentration of formamide from 25% to 50% greatly improves the robustness of the hybridization process.

The presence of formamide in the hybridization buffer increases specificity, avoiding hybridization of sequences with single-base differences [35]. Moreover, it is known that formamide reduces the melting temperature of DNA via the formation of H-bonds competing with the H-bonds between base pairs [36]. This results in improved hybridization since the secondary structure of the single stranded DNA probe is disfavored [37]. The obtained results show that the use of 50 v/v% of formamide in the hybridization buffer and a temperature close to physiological temperature (35 °C) play a pivotal role in the hybridization process.

3.1.3. Hexaethylene glycol backfilling experiments

In the previous section, the optimization of hybridization conditions was discussed. These conditions were applied to a new series of experiments, where a DNA probe with an immobilized HEG spacer (DNA probe 2) was introduced. In a next step, a HEG layer was adsorbed to the surface (i.e. backfilling) with the purpose of avoiding non-specific binding of the complementary DNA. The HEG spacer of the DNA probe makes sure that there is enough space in between the surface and the DNA probe for the backfilled HEG chains to adsorb to the surface. In Table 1, the resonance wavelength shifts observed after backfilling in function of the HEG concentration are shown. For concentrations up to 0.1 mg/ml HEG, the wavelength shifts are more or less constant ($p > 0.1$). When applying higher HEG concentrations, the amount of adsorbed HEG increases significantly ($p < 0.005$).

After backfilling with HEG, a solution of 10 nM complementary DNA was flowed over the ring resonators. The net wavelength shifts of this hybridization step, as a function of the HEG concentration, are also presented in Table 1. Compared to hybridization without a previous backfilling step, the wavelength shift is halved at lower concentrations of HEG ($p < 0.05$). The anti-fouling effect of the adsorbed HEG layer makes sure that the observed wavelength shift can only be attributed to hybridization of complementary DNA, excluding non-specific adsorption. When higher concentrations of HEG were applied, a large increase (9-fold, $p < 0.001$) of the wavelength shift after hybridization was observed compared to the lower HEG concentrations (a 4-fold increase when comparing to hybridization in the absence of HEG, $p < 0.001$). This implies that when backfilling the surface with higher concentrations of HEG, a second effect, apart from the lowering of non-specific adsorption, is occurring, which is beneficial for the hybridization efficiency. This could possibly be explained by an improved orientation of the DNA probe. If the orientation of the DNA probe on the surface is considered, it is reasonable to suppose that the covalently bound DNA probe will fold towards the silicon nitride surface and adsorb to it. This leads to an unfavorable orientation of the DNA probe and inefficient hybridization. This phenomenon has already been inves-

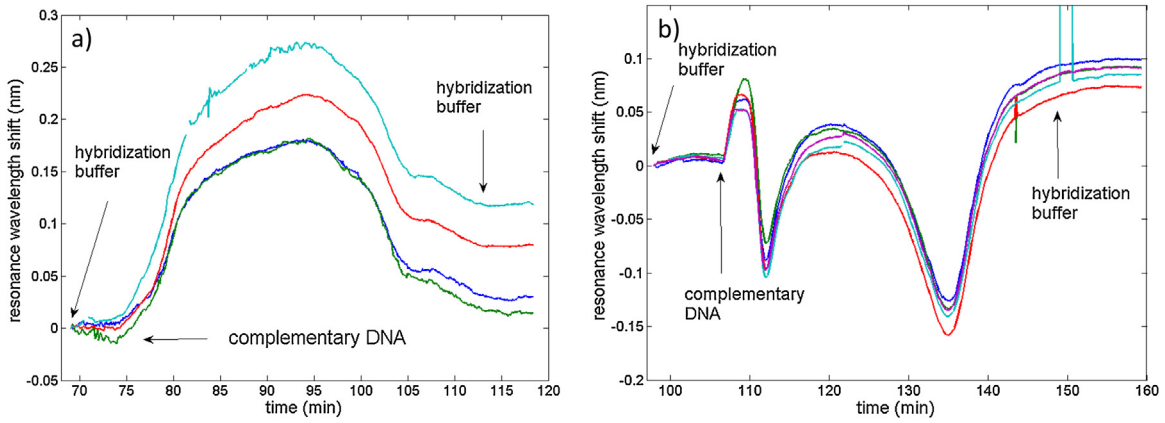

Fig. 3. Binding curves of hybridization of 10 nM complementary DNA in (a) 25 v/v% and (b) 50 v/v% of formamide in PBS pH 7.4 at 35 °C.

tigated on gold surfaces by Herne and Tarlov [38]. Since DNA can also adsorb to silicon surfaces [28,39], a similar effect is likely to happen in this case. The improvement of the single stranded DNA probe orientation has been studied intensively in SPR applications, using mercaptohexanol [38,40] or polyethylene glycol [32,41]. If the orientation of the DNA probe is improved, more single stranded DNA will be available for hybridization with the complementary DNA, explaining the large increase in wavelength shift at higher HEG concentrations. The exact orientation will be studied in section 3.2 with the dual polarization technique. In order to derive an estimation for the detection limit, we must compare the wavelength shift to the minimal detectable wavelength shift of the system determined as 0.6 pm [42]. A 10 nM complementary DNA concentration with a 1 mg/ml HEG backfilling generates a wavelength shift of 361.0 pm. Assuming linearity, a fair assumption considering the reported 3 orders of magnitude linear domain for a DNA assay on a similar microring platform [43], a theoretical detection limit of 17 pM is obtained. Comparing this to literature we find that on very similar labelfree SOI microring resonator platforms a DNA detection limit of 2 nM is reported by Qavi [43] and a tmRNA detection limit of 0.5 pM is reported by Scheler [44]. Using a liquid core optical ring resonator, a detection limit of 10 pM was demonstrated by Suter [45].

Next to an improved efficiency, we also observe an improved robustness due to backfilling with HEG. As before, the biochemical robustness can be studied by quantifying the relative standard deviations on the binding curves. Without backfilling, the relative standard deviation amounts to 0.43. In the case of 1 mg/ml HEG backfilling, the relative standard deviation amounts to 0.06. This improvement can be appreciated by observing Fig. 4. A second element also shows the improved robustness: the transient on the binding curves. In Fig. 4(a) (no backfilling) we observe a considerably more complex hybridization curve, possibly attributed to continuous re-orientation of the DNA probes during the hybridization process. This complexity is absent in Fig. 4(b), where a 1 mg/ml HEG backfilling was applied.

In conclusion we can state that the addition of the anti-fouling HEG does not only lower non-specific binding but also increases the hybridization efficiency, as well as improving the robustness of the assay.

3.2. Dual polarization measurements

The hypothesis that the HEG chains re-orient the DNA strands can be verified with the dual polarization technique. In Fig. 5(a), the resonant wavelength shifts of a TE and a TM mode, which are tracked simultaneously in a single ring, are shown. The sensorgram starts with a buffer switch from ethanol to PBS after binding of the HyNic Silane. Afterwards, a clear positive net shift is observable for the DNA probe, amounting to 87 pm for TE and 475 pm for TM mode. The net shift due to the HEG probe amounts to 13 pm for TE and 103 pm for TM mode. These positive shifts indicate that mass is deposited in both cases. Comparing these numbers to the measured shifts of the DNA probe and the HEG polymer of the TE polarization in the single polarization microring resonators of the previous section, we see that the shift of the TE mode is lower. As mentioned in section 2.3 this can be attributed to the planarization process. On the other hand, the shift of the TM mode is substantially higher, as expected.

These shifts can now be solved to a thickness and density profile, shown in Fig. 5(b) and (c). To compute these characteristics of the stack, it is required to perform simulations with the correct refractive index of the bulk fluid [33]. This bulk fluid is PBS, of which the refractive index is measured to be 1.316 using the wavelength shift of the microring resonator when switching from water to PBS. The thickness and refractive indices of the complete stack after silanization, attachment of the DNA probe and adsorption of HEG are indicated on Fig. 5 as well.

The mass fraction m_l of the layer containing the silane and the DNA probe can be obtained with the following equation:

$$m_l = \frac{n - n_b}{n_{DNA} - n_b} \quad (1)$$

Here, n is the refractive index of the layer on top of the microring, as obtained by the dual polarization technique, n_b is the refractive index of the bulk fluid and n_{DNA} is an average refractive index of the dry DNA molecules and the dry HyNic Silane. This equation is obtained via [46]. A value for the refractive index of DNA was reported as 1.465 at a wavelength of 632.8 nm. We assume that the refractive index of the silane is similar to the refractive index of DNA, which is reasonable, but might introduce small numerical errors [46]. Correcting this term for dispersion [47] we obtain a value of 1.452 for the dry refractive index. With a measured refractive index after attachment of the DNA probe of 1.380, we obtain a mass fraction of the silane + probe layer of 47%.

Looking at the thickness evolution, we observe an increase from 8.71 nm to 12.96 nm due to addition of HEG. Since DNA probe 2 has a HEG spacer attached to it is as well, the size of the HEG molecule is smaller than the size of the stack after attaching the DNA probe. Also, HEG is expected to adsorb to the surface [32] and thus the increase of the thickness of the stack must be attributed to a reorientation of the DNA probes in a more upright position. At the same time we observe a decrease of the refractive index, which implies a decrease of the mass concentration in the stack as shown by equation 1. Although the addition of HEG should increase the mass in

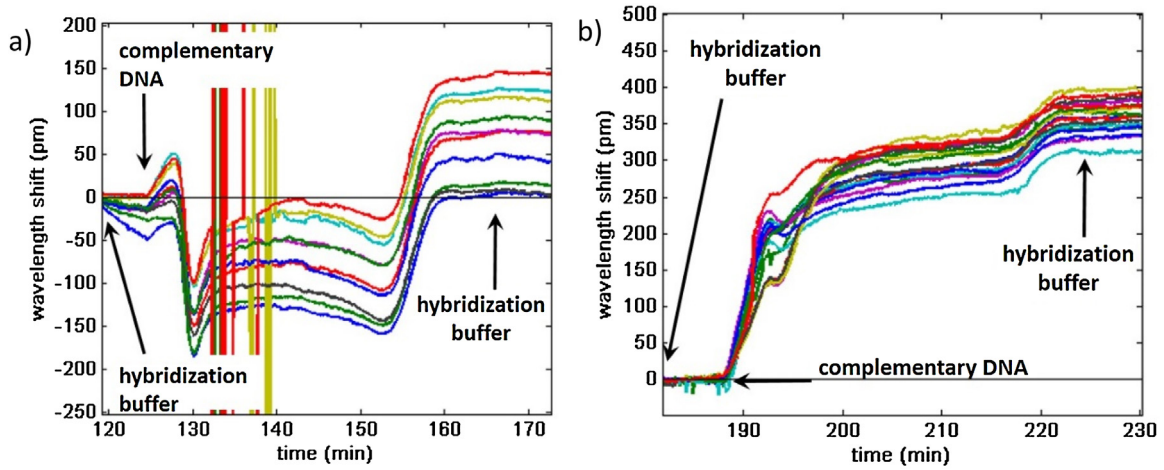

Fig. 4. Binding curve representing the resonance wavelength shift during hybridization of 10 nM complementary DNA in 50 v/v% formamide in PBS pH 7.4 at 35 °C. (a) Hybridization without backfilling, (b) Hybridization following a backfilling step with 1 mg/ml HEG.

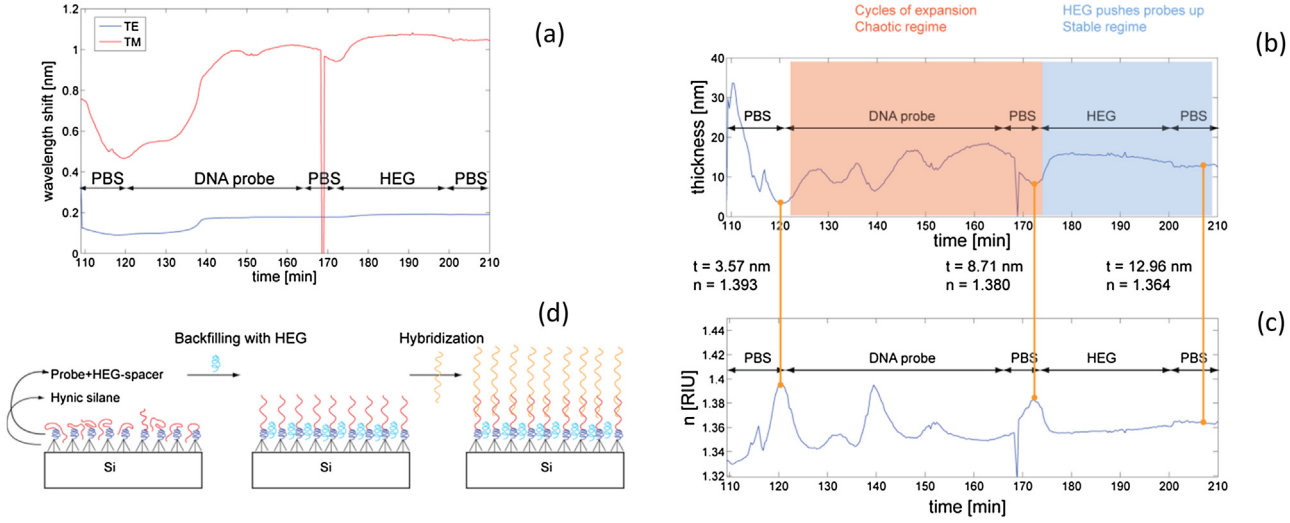

Fig. 5. (a) Wavelength shift of the TE and TM polarized modes in the microring resonator when DNA probe and HEG polymer are flowed over the sensor. The sensor surface is first silanized using a HyNic silane. The wavelength shifts are solved to (b) a thickness profile and (c) a refractive index profile of the bio-stack. This gives information on the orientation of the DNA probes, illustrated on (d). We see that the HEG adsorbs to the surface and pushes the DNA probes in a more upright position, facilitating the subsequent hybridization.

the stack, the unfolding of the DNA molecules is such that it overcompensates this and the mass concentration in this thicker stack decreases. A second observation is that the thickness of the stack is much more stable during the streaming of the HEG molecules than during the streaming of the DNA probe, implying that HEG indeed has a stabilizing function on the DNA probe layer. The hybridization protocol with HEG backfilling together with the DNA reorientation is illustrated in Fig. 5(d).

The thickness profile during the DNA probe attachment shows the level of complexity that is associated with the attachment of DNA probes as several cycles of extension and densification are observed. Consulting literature for an indication of the thickness of a DNA probe layer results in a wide range in the reported thickness. A layer thinner than 1 nm is reported in [46,48] for a 19-mer and a 26-mer strand, where it is concluded that the DNA molecules attach to the surface with its long axis parallel via multiple points. On the contrary, an almost fully extended probe layer of 16.6 nm for a 25-mer strand is reported in [49]. Therefore, we conclude that the 40-mer probe layer is in (partially) upright position, facilitating hybridization.

These results show that the addition of the HEG molecules indeed reorient the DNA strands in a more favorable way, as was hypothesized in the previous section. This reorientation has a positive impact on the robustness, as well as on the hybridization, as shown with the single polarization measurements in the previous section.

3.3. Surface characterization

In order to confirm the deposition of the different molecules on the microring surface during the sensing experiments, we performed similar modification steps on non-patterned silicon nitride substrates. Such substrates allowed us to characterize the modified surface with SCA (determination of the surface wettability) and XPS analysis (determination of the atomic surface composition). The SCA results or water contact angles are shown in Table 2. After simultaneous cleaning and oxidizing the surface by an oxygen plasma treatment, a hydrophylic surface is obtained. This oxidation is necessary to ensure an efficient silanization reaction in the next step. After silanization, the contact angle increases only slightly

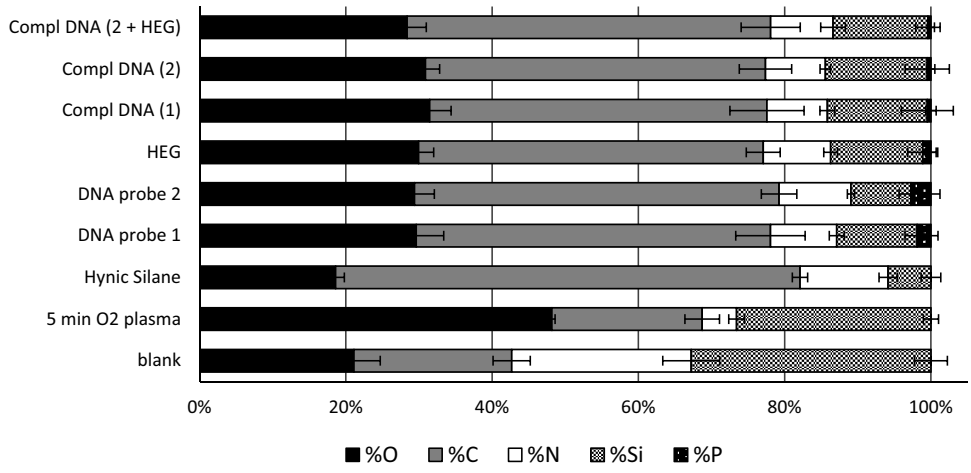

Fig. 6. Atomic surface compositions of the silicon nitride surface after each reaction step, as determined by XPS.

Table 2
Static contact angles of the silicon nitride surfaces after each reaction step.

	Static contact angle (°)	Standard deviation (°)
Blank	38.8	5.2
5 min O_2 plasma	0.0	0.0
Hynic Silane	4.9	3.5
DNA probe 1	40.5	9.8
DNA probe 2	36.8	11.5
HEG	45.0	6.1
Compl DNA (1)	46.2	10.5
Compl DNA (2)	54.3	13.5
Compl DNA (2 + HEG)	53.1	16.0

($p > 0.05$), indicating the surface is still quite hydrophilic. Coupling of the DNA probe, backfilling with HEG and subsequent hybridization of complementary DNA leads to contact angles ranging from 36 to 54°. These results clearly indicate the deposition of molecules onto the silanized surface ($p < 0.05$) but the different layers cannot be distinguished ($p > 0.05$) Therefore we looked closer into the atomic surface compositions measured by XPS (Fig. 6). Compared to the blank, oxygen plasma treatment leads to an increased oxygen and a decreased nitrogen content, indicating that the surface was indeed oxidized ($p < 0.01$). Silanization with HyNic Silane results in a high carbon and an increased nitrogen content ($p < 0.01$). Since the HyNic Silane molecule is carbon based and contains nitrogen, the reaction shows to be successful. Moreover, the decrease of silicon implies that the silicon surface is covered. After attachment of the DNA probes the surface composition changes significantly ($p < 0.01$), but after further backfilling and hybridization, the elemental composition stays more or less constant ($p > 0.05$). The observed amount of phosphorus can be explained by the presence of phosphate groups in DNA sequences. Despite the fact that even with XPS analysis no significant distinction can be made between the DNA, HEG and complementary DNA deposition, the obtained results were in line with the sensing data from Section 3.1, confirming the attachment of DNA, HEG and complementary DNA.

4. Conclusion

This work describes the optimization of the hybridization conditions of DNA sequences on microring detection systems. In a first range of experiments, we showed that the addition of formamide (50 v/v%) to the hybridization buffer improves the robustness of the hybridization protocol by (insert sigma). Furthermore, we only observed hybridization when the temperature is close to the physiological value. In a second range of experiments, we examined the influence of the addition of a HEG layer. Here, we observed the anti-fouling characteristic of HEG by a decrease in the non-specific binding, as well as a four times increase in detection limit when the HEG concentration exceeds 1 mg/ml. By performing a third range of experiments with the novel dual polarization technique, we could confirm the hypothesis that the HEG backfilling pushes the DNA probes in a more upright position, hence improving the hybridization efficiency. These last experiments also show the stabilizing effect of the HEG backfilling method. In a last part, we were able to confirm the different steps in the microring sensing experiments. Therefore we determined the surface wettability and surface composition after each modification step by means of SCA and XPS analysis

Acknowledgements

This work was performed within the framework of the RAPP-ID IMI-project funded by the European Union and EFPIA-partners (www.rapp-id.eu). The authors would also like to acknowledge the financial support of the UGent Multidisciplinary Research Partnership Nano- and Biophotonics. Peter Dubruel would like to thank the Hercules Foundation (grant AUGE09025).

References

[1] V. Scognamiglio, et al., Biosensing technology for sustainable foor safety, Trends Anal. Chem. 62 (2014) 1–10.
[2] S. Song, H. Xu, C. Fan, Potential diagnostic applications of biosensors: current and future directions, Int. J. Nanomed. 1 (2006) 433–440.
[3] M.A. Arugula, A. Simonian, Novel trends in affinity biosensors: current challenges and perpectives, Meas. Sci. Technol. 25 (2014) (032001).
[4] S. Li, et al., An automatic high-throughput single nucleotide polymorphism genotyping approach based on universal tagged arrays and magnetic nanoparticles, J. Biomed. Nanotechnol. 3 (2013) 689–698.
[5] A.M. Goncalves, et al., Trends in Protein-Based Biosensor Assemblies for Drug Screening and Pharmaceutical Kinetic Studies, Molecules 19 (2014) 12461–12485.
[6] I.N. Okeke, et al., Diagnostics as essential tools for containing antibacterial resistance, Drug Resist. Updat. 14 (2011) 95–106.
[7] R.T. Ranasinghe, T. Brown, Ultrasensitive fluorescence-based methods for nucleic acid detection: towards amplification-free genetic analysis, Chem. Commun. 47 (2011) 3717–3735.
[8] J.L. Arlett, E.B. Myers, M.L. Roukes, Comparative advantages of mechanical biosensors, Nat. Nanotechnol. 6 (2011) 203–215.
[9] Y.-P. Ho, et al., Multiplexed hybridization detection with multicolor colocalization of quantum dot nanoprobes, Nano Lett. 5 (2005) 1693–1697.
[10] A. Yalcin, et al., Optical sensing of biomolecules using microring resonators, IEEE J. Sel. Top. Quantum Electron. 12 (2006) 148–155.
[11] A. Ramachandran, et al., A universal biosensing platform based on optical micro-ring resonators, Biosens. Bioelectron. 23 (2008) 939–944.

[12] D.-X. Xu, et al., Folded cavity SOI microring sensors for high sensitivity and real time measurement of biomolecular binding, Opt. Express 16 (2008) 15137–15148.
[13] K. De Vos, et al., Multiplexed antibody detection with an array of silicon-on-Insulator microring resonators, IEEE Photonics J. 1 (2009) 225–235.
[14] A.L. Washburn, et al., Quantitative, label-free detection of five protein biomarkers using multiplexed arrays of silicon photonic microring resonators, Anal. Chem. 82 (2011) 69–72.
[15] Y. Shin, et al., Chemical Label-free methylation specific sensor based on silicon microring resonators for detection and quantification of DNA methylation biomarkers in bladder cancer, Sens. Actuators: B. Chem. 177 (2013) 404–411.
[16] A.J. Qavi, et al., Multiplexed detection and label-free quantitation of microRNAs using arrays of silicon photonic microring resonators, Angewandte Chemie 49 (2010) 4608–4611.
[17] C. Ciminelli, et al., High performance SOI microring resonator for biochemical sensing, Opt. Laser Technol. 59 (2014) 60–67.
[18] M.S. McClellan, et al., Label-free virus detection using silicon photonic microring resonators, Biosens. Bioelectron. 31 (2014) 388–392.
[19] S. Janz, et al., Photonic wire biosensor microarray chip and instrumentation with application to serotyping of Escherichia coli isolates, Opt. Express 21 (2013) 3243–3245.
[20] S. Wang, et al., Integrated microring resonator biosensors for monitoring cell growth and detection of toxic chemicals in water, Biosens. Bioelectron. 24 (2009) 3061–3066.
[21] C. Sirawattananon, et al., Analytical vernier effects of a PANDA ring resonator for microforce sensing application, IEEE Trans. Nanotechnol. 11 (2012) 707–712.
[22] Z. Zhou, H. Yi, Silicon microring sensors, Proceedings SPIE Laser Reson. Microresonators Beam Control XIV 8236 (2012) 1–10.
[23] B.W. Biggs, H.K. Hunt, A.M. Armani, Selective patterning of Si-based biosensor surfaces using isotropic silicon etchants, J. Colloid Interface Sci. 369 (2012) 477–481.
[24] J.-Y. Byeon, F.T. Limpoco, R.C. Bailey, Efficient bioconjugation of protein capture agents to biosensor surfaces using aniline-catalyzed hydrazone ligation, Langmuir 26 (19) (2010) 15430–15435.
[25] A.J. Qavi, et al., Anti-DNA:RNA antibodies and silicon photonic microring resonators: increased sensitivity for multiplexed microRNA detection, Anal. Chem. 83 (2011) 5949–5956.
[26] Y.L. Jeyachandran, et al., Efficiency of blocking of non-specific interaction of different proteins by BSA adsorbed on hydrophobic and hydrophilic surfaces, J. Colloid Interface Sci. 341 (2010) 136–142.
[27] S. Chen, et al., Surface hydration: principles and applications toward low-fouling/nonfouling biomaterials, Polymer 51 (2010) 5283–5293.
[28] A. Cattani-Scholz, et al., PNA-PEG modified silicon platforms as functional bio-Interfaces for applications in DNA microarrays and biosensors, Biomacromolecules 10 (2009) 489–496.
[29] A.R. Lokanathan, et al., Mixed poly(ethylene glycol) and oligo(ethylene glycol) layers on gold as nonfouling surfaces created by backfilling, Biointerphases 6 (2011) 180–188.
[30] K. Uchida, et al., Creation of a mixed poly(ethylene glycol) tethered-chain surface for preventing the nonspecific adsorption of proteins and peptides, Biointerphases 2 (4) (2007) 126–130.
[31] K. De Vos, et al., SOI optical microring resonator with poly(ethylene glycol) polymer brush for label-free biosensor applications, Biosens. Bioelectron. 24 (2009) 2528–2533.
[32] K.P.F. Janssen, et al., Enabling fiber optic serotyping of pathogenic bacteria through improved anti-fouling functional surfaces, Nanotechnology 23 (2012) 235503.
[33] J.-W. Hoste, et al., Conformational analysis of proteins with a dual polarisation silicon microring, Opt. Express 22 (2014) 2807–2820.
[34] F. Dahl, et al., Circle-to-circle amplification for precise and sensitive DNA analysis, Proc. Natl. Acad. Sci. U. S. A. 101 (13) (2004) 4548–4553.
[35] A.J. Qavi, R.C. Bailey, Multiplexed detection and label-Free quantitation of MicroRNAs using arrays of silicon photonic microring resonators, Angew. Chem. Int. Ed. 49 (2010) 4608–4611.
[36] R.D. Blake, S.G. Delcourt, Thermodynamic effects of formamide on DNA stability, Nucleic Acids Res. 24 (11) (1996) 2095–2103.
[37] J. Fuchs, et al., Effects of formamide on the thermal stability of DNA duplexes on biochips, Anal. Biochem. 397 (2010) 132–134.
[38] T.M. Herne, M.J. Tarlov, Characterization of DNA probes immobilized on gold surfaces, J. Am. Chem. Soc. 119 (1997) 8916–8920.
[39] V. Dugas, et al., Immobilization of single-stranded DNA fragments to solid surfaces and their repeatable specific hybridization: covalent binding or adsorption? Sens. Actuators B 101 (2004) 112–121.
[40] A.W. Peterson, L.K. Wolf, R.M. Georgiadis, Hybridization of mismatched or partially matched DNA at surfaces, J. Am. Chem. Soc. 124 (2002) 14601–14607.
[41] C. Boozer, S. Chen, S. Jiang, Controlling DNA orientation on mixed ssDNA/OEG SAMs, Langmuir 22 (2006) 4694–4698.
[42] S. Werquin, Optimizations of a Ring Resonator Biosensor Platform for Applications in DNA Detection PhD Thesis, Ghent University, 2015.
[43] A.J. Qavi, et al., Isothermal discrimination of single-nucleotide polymorphisms via Real-Time kinetic desorption and label-free detection of DNA using silicon photonic microring resonator arrays, Anal. Chem. 83 (2012) 6827–6833.
[44] O. Scheler, et al., Label-free, multiplexed detection of baterial tmRNA using silicon photonic microring resonators, Biosens. Bioelectron. 36 (2013) 56–61.
[45] J.D. Suter, et al., Label-Free quantitative DNA detection using the liquid core optical ring resonator, Biosens. Bioelectron. 23 (2008) 1–21.
[46] B. Lillis, et al., Dual polarisation interferometry characterisation of DNA immobilisation and hybridisation detection on a silanised support, Biosens. Bioelectron. 21 (2006) 1459–1467.
[47] A. Samoc, et al., Refractive-index anisotropy and optical dispersion in films of deoxyribonucleic acid, J. Appl. Polym. Sci. 105 (2007) 236–245.
[48] J.L. Lopez-Paz, et al., Direct and label-free monitoring oligonucleotide immobilization, non-specific binding and DNA recognition, Sens. Actuators B 192 (2014) 221–228.
[49] K.A. Peterlinz, R.M. Georgiadis, T.M. Herne, M.J. Tarlov, Observation of hybridization and dehybridization of thiol-tethered DNA using two-color surface plasmon resonance spectroscopy, J. Am. Chem. Soc. 7863 (1997) 3401–3402.